Auroral particle acceleration by strong double layers: The upward current region

R. E. Ergun,[1] L. Andersson, D. Main, and Y.-J. Su
Laboratory for Atmospheric and Space Physics, University of Colorado, Boulder, Colorado, USA

D. L. Newman and M. V. Goldman
Center for Integrated Plasma Studies, University of Colorado, Boulder, Colorado, USA

C. W. Carlson, A. J. Hull, J. P. McFadden, and F. S. Mozer
Space Sciences Laboratory, University of California, Berkeley, California, USA

Received 16 April 2004; revised 30 June 2004; accepted 26 August 2004; published 24 December 2004.

[1] Satellite observations have established that parallel electric fields of both upward and downward current regions of the aurora are supported, at least in part, by strong double layers. The purpose of this article is to examine the role of double layers in auroral electron acceleration using direct measurements of parallel electric fields and the accompanying particle distributions, electrostatic waves, and nonlinear structures; the concentration is on the upward current region. Direct observations of the ionospheric boundary of the auroral cavity suggest that a stationary, oblique double layer carries a substantial, albeit a minority fraction ($\sim$10% to $\sim$50%) of the auroral potential. An order of magnitude density gradient results in an asymmetric electric field signature. Oblique double layers with amplitudes greater than 100 mV/m have been verified in $\sim$3% and may occur in up to 11% of auroral cavity crossings, so it is feasible that strong double layers are a principal acceleration mechanism. In this article we also present a second type of double layer that has a symmetric electric field signature and is seen inside of the auroral cavity. These structures are a possible signature of a midcavity or high-altitude acceleration mechanism. Numerical solutions of the Vlasov-Poisson equations support the possibility of midcavity double layers and indicate that trapped electrons can play an important role in the double-layer structure. *INDEX TERMS:* 7807 Space Plasma Physics: Charged particle motion and acceleration; 7839 Space Plasma Physics: Nonlinear phenomena; 2704 Magnetospheric Physics: Auroral phenomena (2407); 2712 Magnetospheric Physics: Electric fields (2411); 2716 Magnetospheric Physics: Energetic particles, precipitating; *KEYWORDS:* auroral acceleration, double layers, parallel electric fields

Citation: Ergun, R. E., L. Andersson, D. Main, Y.-J. Su, D. L. Newman, M. V. Goldman, C. W. Carlson, A. J. Hull, J. P. McFadden, and F. S. Moser (2004), Auroral particle acceleration by strong double layers: The upward current region, *J. Geophys. Res.*, *109*, A12220, doi:10.1029/2004JA010545.

1. Introduction

[2] Ever since the realization that earthward accelerated electrons carrying upward currents cause visible auroral arcs, a prime focus in auroral science has been to identify the physical process that accelerates auroral electrons. Electron distributions measured from sounding rockets [*McIlwain*, 1960] gave the first indication that the acceleration process of the quiescent arc was from a quasi-static parallel electric field [*Evans*, 1974]. This idea was reinforced further by satellite observations of antiearthward ion beams [*Shelley et al.*, 1976] and by observations of quasi-static perpendicular electric field structures [*Mozer et al.*, 1977; *Block et al.*, 1987]. The ion and electric field observations confined the location of the parallel electric fields to be, in most cases, near Earth, between $\sim$1/2 and $\sim$2 R_E in altitude. The parallel electric fields in the upward current region are associated with field-aligned currents at the boundary between the cold, dense, ionospheric plasma (T_e < 1 eV, $n_e \sim 10^1$–10^5 cm^{-3}) and the hot, tenuous, magnetospheric plasma ($T_e \sim$ 500 eV, $n_e \sim$ 1 cm^{-3}). It is believed that parallel electric fields are forced upon the system by a combination of strong upward (antiearthward) currents and a substantial magnetic mirror ratio ($\sim$400) between the source electron population in the tail of the Earth's magnetosphere and the visible arc in the ionosphere [*Knight*, 1973; *Fridman and Lemaire*, 1980]. Theoretical treatments of the self-consistent structure of the parallel electric fields include weak double layers [*Temerin et al.*, 1982], strong double layers [*Block*, 1972], anomalous resistivity [*Hudson and Mozer*, 1978], and parallel electric

[1]Also at Department of Astrophysical and Planetary Sciences, University of Colorado, Boulder, Colorado, USA.

0148-0227/04/2004JA010545$09.00

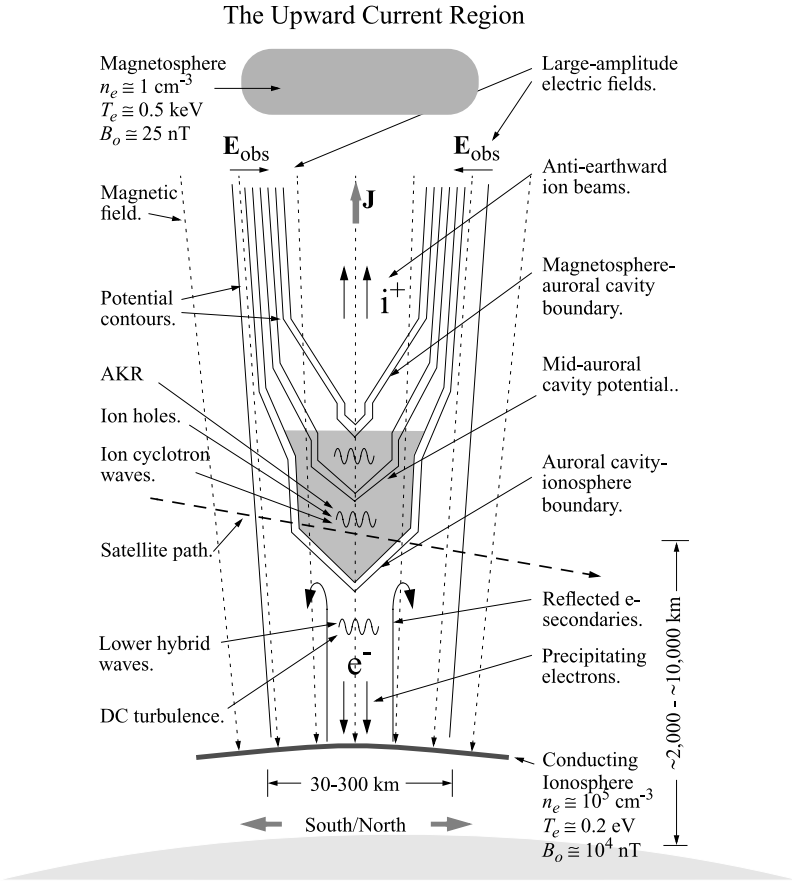

Figure 1. A simplified cartoon of the upward current region of the aurora. The potential contours (solid lines) indicate a low-altitude and high-altitude acceleration region with the auroral cavity in between.

fields associated with ion cyclotron waves [*Ishiguro et al.*, 1997].

[3] Direct observations of localized, large-amplitude parallel electric fields and the associated particle distributions have been made in the upward current region [*Mozer and Kletzing*, 1998; *Ergun et al.*, 2002a; *Hull et al.*, 2003a, 2003b]. The large-amplitude parallel electric fields, for the most part, have been seen at the boundary between the ionosphere-dominated plasma and the auroral cavity and contain roughly 10–50% of the auroral potential [*Mozer and Hull*, 2001; *Ergun et al.*, 2002a]. Numerical solutions of the Vlasov-Poisson equations indicate that the measured electric fields, electron distributions, and ion distributions are consistent with a stationary, oblique double layer [*Ergun et al.*, 2002b]. These observations and analytical treatments argue for the existence of double layers but do not rule out other physical mechanisms.

[4] This article concentrates on the physics of electron acceleration in static auroral structures in the upward current region. Specifically, we concentrate on the role of the strong ($e\Delta\Phi > T_{e,i}$) double layer [*Block*, 1972; *Schamel and Bujarbarua*, 1983]. We use the small number of direct observations of parallel electric fields to argue that the strong double layer may be the dominant mechanism of auroral acceleration at the boundary between the auroral cavity and ionosphere. Furthermore, we present evidence of double layers within the auroral cavity and demonstrate that the electron and ion distributions are consistent with formation of "ion-beam" double layers. An ion-beam double layer can form if the ion-beam density exceeds the density of the hot plasma sheet ions. At higher altitudes where the density of hot plasma sheet ions dominate, double-layer solutions result in highly unstable electron distributions with a depletion of trapped electrons. Such depletions, however, have not been supported by observations so, while possible, a monotonic double layer at rest is unlikely in regions where the plasma sheet ions dominate. These studies indicate that the trapped electron population has an important role the structure of the high-altitude parallel electric field.

2. Overview of the Upward Current Region

[5] Figure 1 displays an oversimplified model of the upward current region derived from many years of auroral research [e.g., *Carlson et al.*, 1998] and large-scale modeling [*Ergun et al.*, 2000]. The dashed lines represent the magnetic field lines, and the solid lines portray potential contours which embody a parallel electric field. The observed net potential drop in the auroral system often is comparable to the large-scale potential predicted from a field-aligned electron current in a mirroring magnetic field [*Knight*, 1973]. However, the spatial distribution of the electric potential along the magnetic flux tube between the ionosphere and the magnetosphere and how it is self-consistently supported are not well established. The location of the auroral potential is generally between $\sim$1/2 and 2 R_E

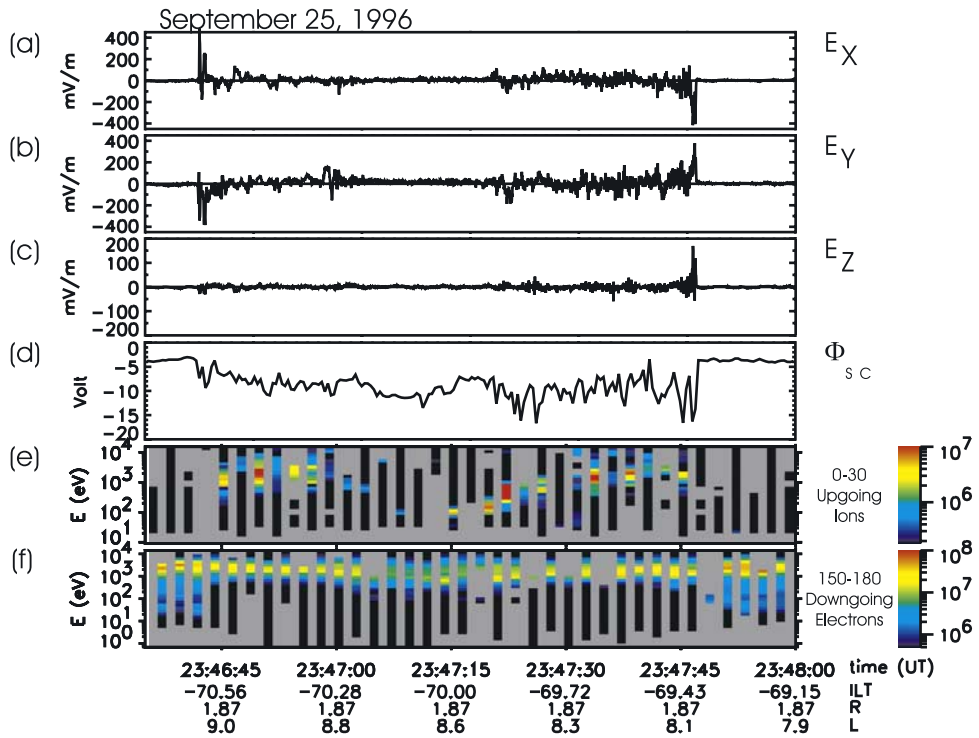

Figure 2. A "textbook" example of a satellite crossing of the auroral cavity in the static upward current region. The data are from the Polar spacecraft. (a and b) Two components of the perpendicular electric field. (c) $E_{||}$. (d) The spacecraft potential. (e) The antiearthward ion energy flux as a function of energy and time. (f) The earthward electron energy flux as a function of energy and time. Adapted from *Hull et al.* [2003b].

in altitude but has been inferred from observations at higher altitudes (>2 R_E) and at altitudes as low as 1000 km [*Haerendel et al.*, 1976; *Klumpar*, 1979; *Reiff et al.*, 1993].

[6] Satellite observations [*Reiff et al.*, 1988; *Burch*, 1988; *Mozer and Hull*, 2001] and quasi-neutral modeling [*Ergun et al.*, 2000] suggest that the parallel electric fields concentrate in at least two locations along the magnetic field line. A low-altitude transition layer is at the boundary between the ionospheric plasma and the tenuous auroral cavity plasma. This boundary layer can carry ~10% to ~50% of the total auroral potential, has been directly observed [*Mozer and Kletzing*, 1998; *Ergun et al.*, 2002a; *Hull et al.*, 2003a, 2003b], and has been characterized as a strong double layer [*Ergun et al.*, 2002b]. Quasi-neutral solutions suggest that a moderate parallel electric field is needed within the auroral cavity to maintain quasi-neutrality and also predict a high-altitude transition layer which carries the majority of the auroral potential. The large-scale, quasi-neutral solutions leave open the possibility that one or more double layers form at high altitudes.

[7] The auroral acceleration region is characterized by strong wave emissions that play an important role in the relaxation of the accelerated electron and ion distributions. On the ionospheric side of the low-altitude transition layer (hereinafter called the auroral cavity–ionosphere boundary), earthward accelerated electron fluxes enter a region of dense ($10–10^5$ cm^{-3}), cold (order of 1 eV) plasma. The resulting electron distributions can have a "bump on tail" instability whereby the "cold" ionospheric plasma dominates the real part of the dispersion and the hot accelerated electrons provide the free energy source. As a result, intense electrostatic whistler emissions [e.g., *Maggs*, 1976] near the lower hybrid frequency, ion cyclotron waves, and broadband low-frequency turbulence are commonly observed immediately below the low-altitude transition layer. Inside of the auroral cavity, an antiearthward ion beam emerges from the low-altitude parallel electric field into the low-density (usually <1 cm^{-3}) auroral cavity. The ion density is dominated by the ion beam and a smaller contribution from the hot (several keV) plasma sheet ions. Several strong instabilities can lead to the observed large-amplitude ion cyclotron waves including an ion-ion drift instability [e.g., *Roth et al.*, 1989], shear instabilities [e.g., *Gavrishchaka et al.*, 2000], and drift instabilities [e.g., *Chaston et al.*, 2002]. These waves significantly modify both the electron and ion distributions.

3. Auroral Cavity–Ionosphere Boundary Layer

[8] The auroral cavity–ionosphere boundary has been characterized by satellite observations [*Hull et al.*, 2003a]. Roughly 100 verified observations of the parallel electric field of the upward current region crossings have been identified by Polar and FAST satellites. Figures 2 and 3 display observations interpreted as parallel electric fields at an auroral cavity–ionosphere boundary crossing.

3.1. Observations

[9] Figure 2 displays plasma observations from the Polar satellite as it crossed an auroral arc in the Southern

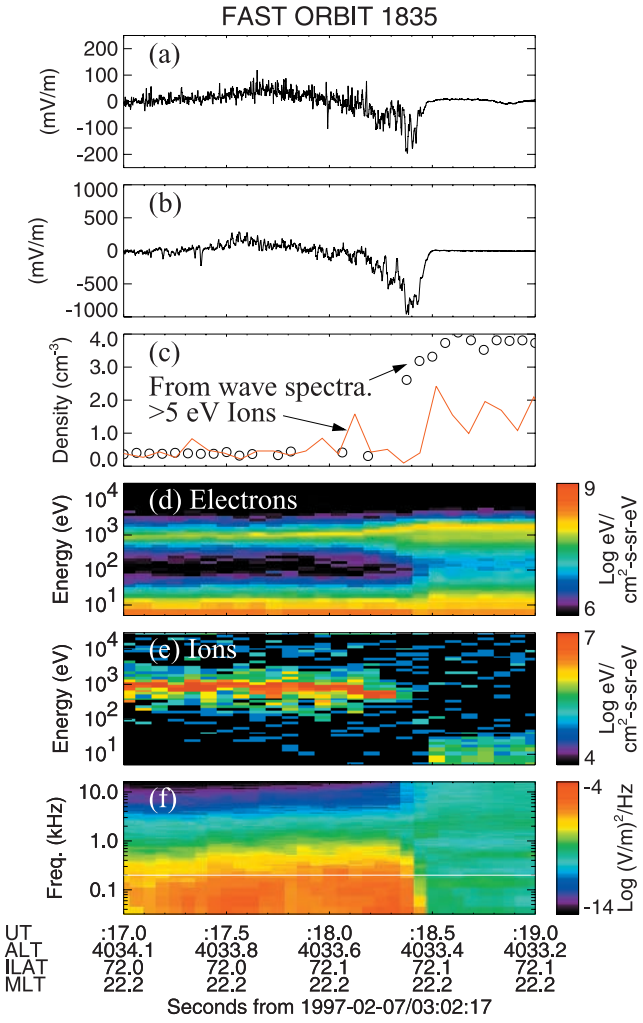

Figure 3. An example of an asymmetric, oblique double layer. (a) $E_{\|}$. (b) $E_{\perp}$. (c) The density of >5 eV ions (red line) and the plasma density estimated from wave characteristics (black circles). (d) The electron energy flux versus energy (vertical axis) and time (horizontal axis). (e) The ion energy flux versus energy (vertical axis) and time (horizontal axis). (f) The wave spectral power density versus frequency (vertical axis) and time (horizontal axis).

Hemisphere. The horizontal axis represents 90 s of time; the satellite was moving from south to north. These observations have been reported earlier [*Hull et al.*, 2003b], so our description is brief. Figures 2a, 2b, and 2c show the vector electric field in a magnetic-field- aligned coordinate system where E_z is the parallel electric field [*Hull et al.*, 2003b]. Figure 2d displays the spacecraft potential, which is a measure of plasma density. Figures 2e and 2f show the up-going ion fluxes and down-going electron fluxes. Up-going electron fluxes (not shown) are present and dominated by mirror electrons, electrons scattered in the ionosphere, and electron secondaries.

[10] Put in the context of the cartoon in Figure 1, the observations in Figure 2 represent a "textbook" example of an auroral cavity crossing in the static upward current region. Downward accelerated electron fluxes (Figure 2f) at ~3 keV are seen throughout the crossing. The spacecraft is outside of the auroral cavity (in the ionospheric plasma) at the beginning of the plot. At ~2346:42 UT a sharp drop in spacecraft potential (Figure 2d) occurs simultaneously with a large-amplitude perpendicular electric field (Figures 2a and 2b), low-frequency electric field turbulence, and anti-earthward ion fluxes (Figure 2e). The energy of the peak electron fluxes decreases. The spacecraft exits from the auroral cavity at ~2347:47 UT with an observational signature that is similar to the cavity entry but with the opposite sign in the perpendicular electric field ($E_{\perp}$).

[11] A parallel electric field ($E_{\|}$) with a peak amplitude of ~150 mV/m (positive is upward in the Southern Hemisphere) is observed at the second crossing of the auroral cavity–ionosphere boundary (Figure 2c at ~2347:47 UT). A variance analysis [*Hull et al.*, 2003b] indicates the electric field is inclined at ~75° with respect to the magnetic field. The thickness of the electric field layer is ~5.7 km (~6 km perpendicular to **B** and ~23 km along **B**). When present, the $E_{\|}$ signature at the auroral cavity–ionosphere boundary often exhibits an asymmetry. The signal changes abruptly on the ionospheric side but slowly relaxes inside of the auroral cavity. The amplitude of the $E_{\|}$ signal, the thickness of the electric field layer, and the asymmetric shape of the signal are in consort with double-layer interpretation [*Ergun et al.*, 2002b].

[12] Figure 3 displays a second set of plasma observations in the auroral acceleration region. These observations are from the Fast Auroral Snapshot (FAST) [*Carlson et al.*, 1998] satellite at ~3700 km in altitude. The data have been reported earlier [*Ergun et al.*, 2002b] so our description, once again, is brief. The horizontal axis in Figure 3 represents 2 s of the evening auroral zone moving from south to north (see Figure 1) during which the satellite traversed approximately 11 km. The satellite is within the auroral cavity in the beginning of the plot and exits into the ionosphere ~0302:18.45 UT.

[13] Figure 3a displays the measured $E_{\|}$ in the dc to 4 kHz frequency range. The $E_{\|}$ signal has a large negative excursion (negative is upward in the Northern Hemisphere) at the auroral cavity–ionosphere boundary (0302:18.4 UT). Figure 3b plots the dc electric field perpendicular to **B** in the direction closest to the spacecraft velocity (positive is mostly northward and nearly parallel to the satellite's velocity). The large negative excursion at ~0302:18.4 UT is a signature of a converging electric field structure as diagrammed in Figure 1.

[14] The plasma density is estimated from two techniques (Figure 3c). The red line represents the density of 5 eV to 25 keV ions. The black circles are the plasma density estimated from plasma wave cutoff [*Ergun et al.*, 1998; *Strangeway et al.*, 1998]. Each of the two estimates has a factor of 2 uncertainty; the uncertainty of the wave cutoff method increases near a boundary with a strong density gradient or in regions of rapidly changing densities. Within the uncertainties, the two values predict ~0.4 cm^{-3} density inside of the cavity. Outside of the auroral cavity, the ionospheric ions may have a significant population less than 5 eV, so the plasma density (~3 cm^{-3}) is best represented by the plasma wave properties (black circles). The large, $O(10)$, change in density is characteristic of the auroral cavity–ionosphere boundary at ~1/2 to 1 R_E altitudes.

[15] The differential electron energy flux is plotted in Figure 3d. The vertical axis represents energy and the color represents electron energy flux summed over all pitch angles. One can see a clear peak in energy flux at energies between ~1 keV and ~2 keV throughout the plot. There are a dearth of electron fluxes below ~1 keV in the auroral cavity (the fluxes below ~100 eV are from spacecraft photoelectrons). Figure 3e displays the ion energy flux in the same format. An ion beam stands out at roughly 1 keV traveling antiearthward. The energy of the peak fluxes of electrons and ions sum to ~2 keV, indicating an enduring net potential of ~2 kV.

[16] Figure 3f displays the electric field spectral power density. Most notable are the intense emissions inside of the auroral cavity near the H+ cyclotron frequency (indicated by a white line). These intense emissions strongly affect the ion fluxes emerging from the parallel electric field of the auroral cavity–ionosphere boundary.

[17] The observations in Figures 2 and 3 and others [*Mozer and Kletzing*, 1998; *Ergun et al.*, 2002a; *Hull et al.*, 2003a, 2003b] are candidates of oblique double layers. $E_{\|}$ and $E_{\perp}$ display similar profiles and are confined to a layer of the order of several λ_D ($\lambda_D \sim 1$ km as determined from the electron properties inside of the auroral cavity). Electric field waveforms and the electron and ion distributions were examined in several events and shown to be consistent with a solution of an asymmetric, stationary, oblique, double layer [*Ergun et al.*, 2002b].

[18] The asymmetric electric field signals in Figures 2 and 3 come from the strong gradient in plasma density at the auroral cavity–ionosphere boundary. The ionospheric side has a strong, confined positive charge layer scaling with the ionospheric Debye length, typically <100 m. There is a moderate, extended negative charge layer on the auroral cavity side, scaling with the auroral cavity Debye length which is O(1 km).

[19] Double layers at the auroral cavity–ionosphere boundary are most often oblique with $|E_{\perp}| > |E_{\|}|$. A planar, oblique double layer can be incorporated in one-dimensional (1-D) BGK modeling [*Ergun et al.*, 2002b], but the physical process that governs the angle of the double-layer normal from **B** ($\alpha = \tan^{-1}(E_{\perp}/E_{\|})$) is not understood. Electron and H^+ motions conserve the fist adiabatic invariant since the double-layer thickness (several λ_D) is much larger than the electron and H^+ gyroradii. If the ion beam is H^+ dominated, then the ion motion is confined to be along **B** so α is not governed by small-scale processes. Rather α could be controlled by the large-scale potential structure. On the other hand, the double-layer thickness can be of the order of the O^+ gyroradius. The motion of O^+ can significantly distort the double structure and may influence α. Furthermore, intense wave emissions within the auroral cavity strongly modify the accelerated ion distributions. These wave emissions may also affect α. Exploration of the 3-D, dynamic solutions of double layers is an area of future research.

[20] The measured double layers are consistent with stationary solutions (with respect to the ionospheric plasma), most significantly, the structures need not be moving along **B**. The Bohm and Langmuir conditions (see *Raadu* [1989] for a review of double layers) are satisfied by an antiearthward drift of the ionospheric ions. The ionospheric ions acquire their antiearthward drift through transverse (to **B**) heating by intense plasma waves and turbulence that is found in the auroral ionosphere. The magnetic mirror force of the transversely heated ions overcomes the gravitational binding force and accelerates the ions antiearthward into the double layer.

[21] The double-layer solution is strongly influenced by the ionospheric secondary electron population. Interestingly, the precipitating electrons (accelerated through the double layer) generate the ionospheric secondary electrons and the plasma waves that heat the ionospheric ions. In essence, the double layer at the auroral cavity–ionosphere boundary creates a self-supporting, steady state environment. The growth and evolution of the auroral cavity–ionosphere double layer is clearly a complex problem than cannot be isolated from the ionospheric response.

3.2. Statistical Argument

[22] A 100-event study on FAST satellite data was used to search for parallel electric fields. An "event" is auroral cavity crossing defined by an antiearthward ion beam that (1) endures for longer than 1 s, (2) has a peak energy flux (ψ) at an energy (ξ) greater than 100 eV, (3) has a minimum energy flux of 10^6 cm^{-2} s^{-1} sr^{-1} in the 22.5° angular sector closest to **B** and is antiearthward, and (4) has $\psi(\xi)$ in the 22.5° sector closest to **B** that is 3 times greater than all other angular sectors except the two closest in angle. All 100 events that satisfied the above definition were in the upward current region (as determined from magnetic field measurements), had a density depletion during the period of the ion beam, had evidence of perpendicular electric field signals at the boundary of the ion beam, and had energetic, precipitating electron fluxes. The ion beam, as defined, is a robust indicator of the auroral cavity at FAST altitudes. Almost all of the crossings were at altitudes within 1000 km of the FAST apogee (4250 km).

[23] In this study, there are 200 crossings (one inbound, one outbound) of the auroral cavity boundary at altitudes where the auroral cavity–ionosphere boundary is expected to be observed. Six of the boundary crossings had verifiable $E_{\|}$ signals. *Ergun et al.* [2002a] discuss the criteria for validating $E_{\|}$ observations, one of which is that the amplitude must be greater than 100 mV/m. All six of the $E_{\|}$ events were consistent with an oblique double layer so at least 3% of the auroral cavity–ionosphere boundary crossings indicate double layers. The FAST study, however, did not verify parallel electric field measurements when $|E_{\|}| < 100$ mV/m or when the electric field instrument may have been saturated by strong wave emissions. Of the boundary crossings where the electric field instrument was not saturated, one can verify that the $E_{\|}$ was consistent with zero on 178 the auroral cavity–ionosphere boundary crossings. Thus it is possible that 22 of 200 crossings (11%) of the auroral cavity–ionosphere boundary crossings have parallel electric fields.

[24] In a separate study, *Hull et al.* [2003a] presented 64 Polar observations of parallel electric fields with amplitudes greater than 25 mV/m representing 2% of all inbound and outbound auroral zone passes. The majority of the events were less than 100 mV/m, even though one of the verification requirements in that study was that the $|E_{\|}|/|E_{\perp}| > 0.2$, a requirement which further eliminates many low-amplitude

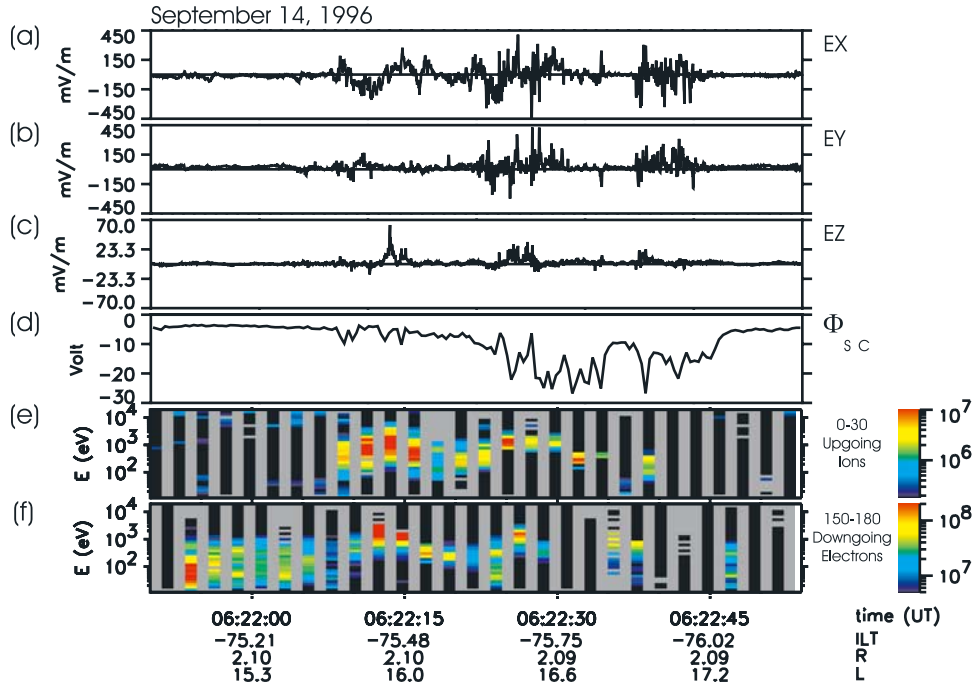

Figure 4. A possible midcavity parallel electric field measured by the Polar spacecraft. (a and b) Two components of the perpendicular electric field. (c) $E_{\|}$. (d) The spacecraft potential. (e) The antiearthward ion energy flux as a function of energy and time. (f) The earthward electron energy flux as a function of energy and time. Adapted from *Hull et al.* [2003a].

events. The Polar observations were, on average, ~1.2 R_E in altitude.

[25] Assuming that the parallel electric field at the auroral cavity–ionosphere boundary is entirely supported by oblique double layers, all with α such that $|E_{\|}|/|E_{\perp}| = 0.4$ [*Hull et al.*, 2003a], the expected number of double layer observations at auroral cavity–ionosphere boundary crossings depends entirely on the geometry of the auroral acceleration region. In rough numbers, the auroral cavity is, on average, ~32 km in half width (north-south) as observed at FAST altitudes in our study (the half width will be less if arcs are not east-west aligned). Given a fixed value α, the vertical extent of the double layers should be, on the average, 80 km (it can be one or more segments) as depicted by Figure 1. One should measure finite $E_{\|}$ in roughly 8% of the auroral cavity boundary crossings (north-south) if one randomly scans an altitude range of 1000 km which includes the lowest-altitude section of the auroral cavity–ionosphere boundary (3250–4250 km in altitude, the range of FAST observations of the cavity in our study). The low-altitude FAST satellite should see a higher rate of occurrence rate of double layers at boundary crossings than does Polar.

[26] Under this entirely geometric argument, the observational occurrence (3–11% on FAST) of double layers allows that the $E_{\|}$ at the auroral cavity–ionosphere boundary could be supported entirely by double layers. Such a statistical argument, of course, is not conclusive. Among the many other sources of error besides poor statistics is that the large-scale structure of the aurora cannot be uniquely determined by the current set of observational data and is certainly more complex than we assume. Nonetheless, we can conclude that double layers have been observed at the auroral cavity–ionosphere boundary and that their observational occurrence is high enough for double layers to be a dominant physical mechanism.

4. Midcavity Double Layers

[27] The potential across the auroral cavity–ionosphere boundary is a few tens of percent of the auroral potential. Thus the majority of the auroral potential is either within the auroral cavity or at a high-altitude transition layer between the auroral cavity and the magnetospheric plasma [*Mozer and Kletzing*, 1998; *Ergun et al.*, 2000]. The nature of the auroral potential inside of the auroral cavity and at the high-altitude transition layer is largely undetermined. In this section we explore the role of the double layer inside of the auroral cavity.

4.1. Observations

[28] Figure 4 displays an example of a possible midcavity or high-altitude double layer. The format is nearly identical to that of Figure 2. The Polar spacecraft was traveling from north to south through the southern auroral zone. Its altitude is ~7000 km. It entered the auroral cavity at ~0622:09 UT as evidenced by a large-amplitude signal in $E_{\perp}$ (Figure 4a), a depletion in plasma density (the spacecraft potential, Figure 4d), and the appearance of an antiearthward ion beam (Figure 4e).

[29] An upward directed $E_{\|}$ with amplitude >50 mV/m is seen at ~0622:14 UT. This event is not interpreted as the auroral cavity–ionosphere boundary since an antiearthward ion beam is seen before and after the event (Figure 4e).

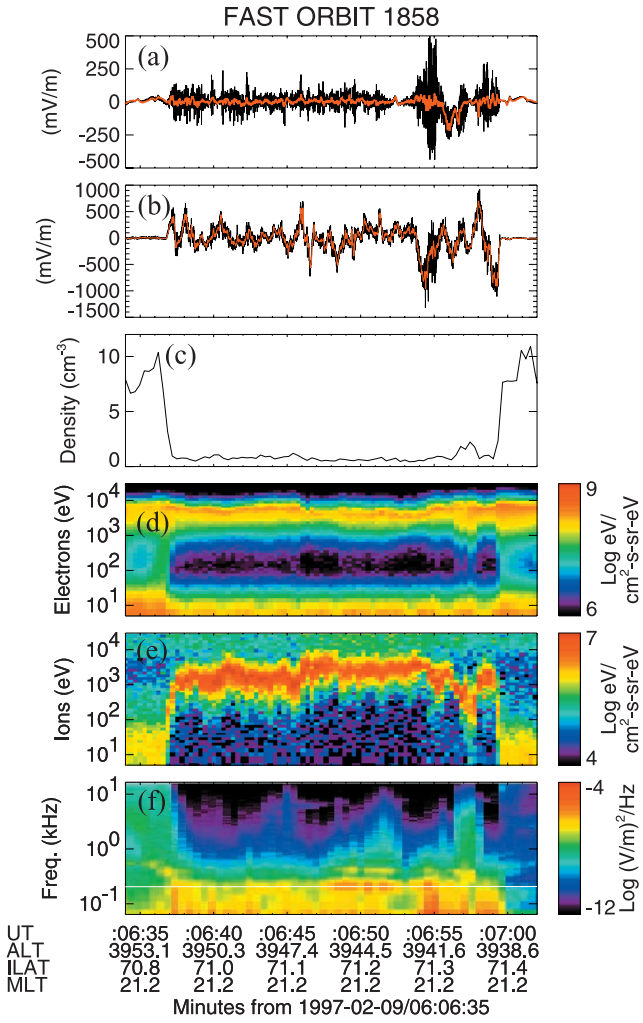

Figure 5. A possible midcavity double layer. (a) $E_{\parallel}$. The black trace is 250-Hz bandwidth. The red trace is 10-Hz bandwidth. (b) $E_{\perp}$. (c) The density of >5 eV ions. (d) The electron energy flux versus energy and time. (e) The ion energy flux versus energy and time. (f) The wave spectral power density versus frequency and time.

Instead, it appears to be a midcavity or high-altitude $E_{\parallel}$ structure. Since the ion and electron distributions are not continuous in time, this interpretation is not conclusive.

[30] Another possible midcavity double layer is plotted in Figure 5. These data are from the FAST satellite at ~3900 km in altitude. The display format is identical to that in Figure 3. The spacecraft, traveling from south to north through the northern aurora, entered the auroral cavity at ~0606:37 UT and exited back into the ionosphere-dominated plasma at ~0606:59 UT. The auroral cavity–ionosphere boundaries are clearly seen in the perpendicular electric field (Figure 5b), the ion density (Figure 5c), the energetic electrons (Figure 5d), and the energetic ions (Figure 5e).

[31] The upward directed $E_{\parallel}$ is seen at ~0606:56 UT inside of the auroral cavity. The ion-beam energy (Figure 5e) decreases from ~1.6 keV prior to the $E_{\parallel}$ signal to ~600 eV after the signal. The characteristic energy of the electron fluxes increases from ~2 keV before the event to ~3 keV after the event. The spacecraft appears to be in a region of lower potential before the $E_{\parallel}$ signal and in a region of higher potential after the $E_{\parallel}$ signal. We interpret this event as the spacecraft crossing a midcavity $E_{\parallel}$ since the ion beam persists before and after the $E_{\parallel}$ signal.

[32] The $E_{\parallel}$ event in Figure 5, while at an unusually low altitude, can be used to characterize the auroral cavity electron and ion distributions and theoretically examine the possibility of midcavity double layers. Using a technique analogous to that of an earlier study [*Ergun et al.*, 2002b], the measured electron and ion distributions before the $E_{\parallel}$ signal will be used to characterize the plasma distributions "above midcavity $E_{\parallel}$" (the high-altitude side of a midcavity double layer), and the plasma distributions after the $E_{\parallel}$ signal will be used to characterize the "below midcavity $E_{\parallel}$" (low-altitude side of the double layer). Because of the motion of the spacecraft, the distributions above and below midcavity $E_{\parallel}$ are measured in separate flux tubes, so only the general characteristics are investigated.

4.2. Electron and Ion Distributions

[33] Figures 6a–6d display reduced, 1-D electron and ion distributions (circles) taken above a midcavity $E_{\parallel}$ (Figures 6a and 6b) and below midcavity $E_{\parallel}$ (Figures 6d and 6e). The solid lines are fits to the distributions which are described below. The associated $E_{\parallel}$ signal is plotted at 4-kHz bandwidth in Figure 6c. Figures 6f–6i are reduced, 1-D electron and ion distributions (circles) from another event which was interpreted as a auroral cavity–ionosphere boundary crossing (see *Ergun et al.* [2002b] for a discussion of these distributions). Figure 6 displays a series of electron and ion distributions that we put forth as representative of the progression of electron and ion distributions from the ionosphere to the magnetosphere in the upward current region of the aurora.

[34] The fits of the electron distribution are combinations of a "flat-top" distribution and a drifting Maxwellian. The flat-top distribution is defined as

$$f(v) = f_o e^{-\frac{1}{2}m(v-v_o)^2/\chi_o} \quad (v \geq v_o) \tag{1}$$

$$f(v) = f_o \quad (|v| < v_o)$$

where χ_o characterizes the high-energy part of the distribution (it is distinct from the temperature), m is the particle mass, and v_o is a characteristic velocity determined by fit. The drifting Maxwellian distributions defined as

$$f(v) = f_o e^{-\frac{1}{2}m(v-v_d)^2/kT} \tag{2}$$

where v_d is the drift velocity and T is the temperature. If v_d = 0, equation (2) reduces to a Maxwellian.

[35] Auroral electron distributions have three main constituents including electrons of magnetospheric origin, electrons of ionospheric origin, and trapped electrons. Figure 7 displays 2-D plots of two midcavity electron distributions from Figure 6. The distributions are partitioned into regions that represent the different constituents. Region M are the accelerated electrons from the magnetosphere (plasma sheet), and M_R are the mirrored component. Region I are ionospheric secondaries and scattered primaries, and I_R are reflected from a parallel electric field at high altitude. The region marked as T_{NL} (trapped nonlocally) includes the trapped electrons that

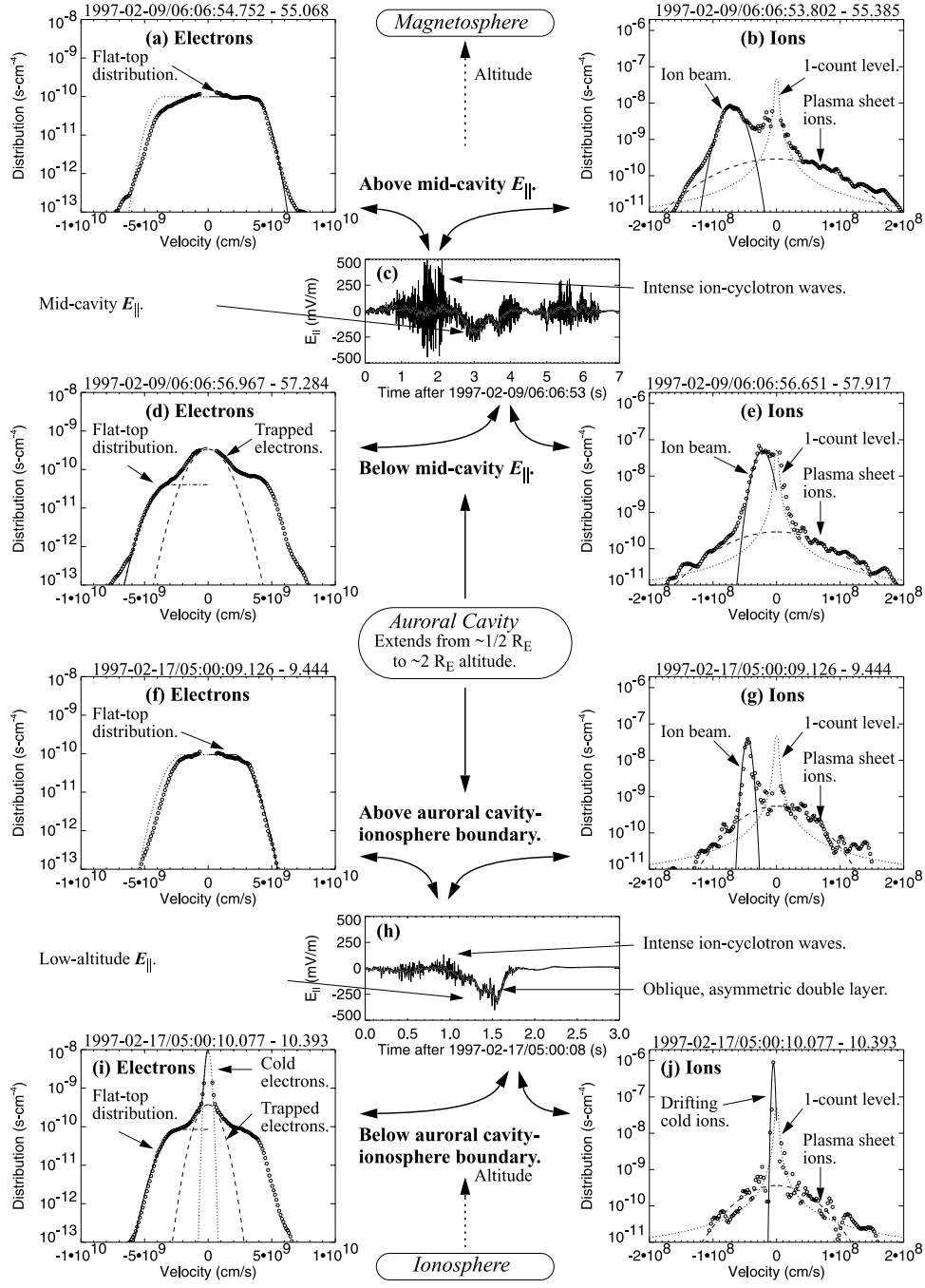

Figure 6. The evolution of electron and ion distributions in the auroral zone. (a) The reduced, 1-D electron distribution measured above the possible midcavity double layer in Figure 5. The electrons fit well to a flat top (equation (1)). (b) A reduced, 1-D ion distribution measured above the midcavity double layer. The ion distribution can be represented by the combination of an ion beam (drifting Maxwellian, equation (2)) and hot plasma sheet ions (Maxwellian). The ion population near $v = 0$ is near the one-count level of the instrument and therefore is not well established. (c) An expanded view of the $E_{||}$ wave signal from Figure 5. The noisy black trace has a frequency range from dc to 250 Hz, and the smooth black trace with white traces above and below indicates the dc to 10-Hz signal. (d) The reduced, 1-D electron distribution measured below the midcavity layer in Figure 5. This distribution fits well to a combination of a flat-top distribution and a Maxwellian core. The Maxwellian core is primarily from trapped electrons. (e) A reduced, 1-D ion distribution measured below the possible midcavity double layer. The ion distribution is fit to a combination of an ion beam (drifting Maxwellian, equation (2)) and hot plasma sheet ions (Maxwellian). The ion drift speed is less than in Figure 6d. (f–j) The electron and ion distributions above and below a double layer at the auroral cavity-ionosphere boundary [*Ergun et al.*, 2002a, 2002b]. The figures are plotted in the same format as in Figures 6a–6e.

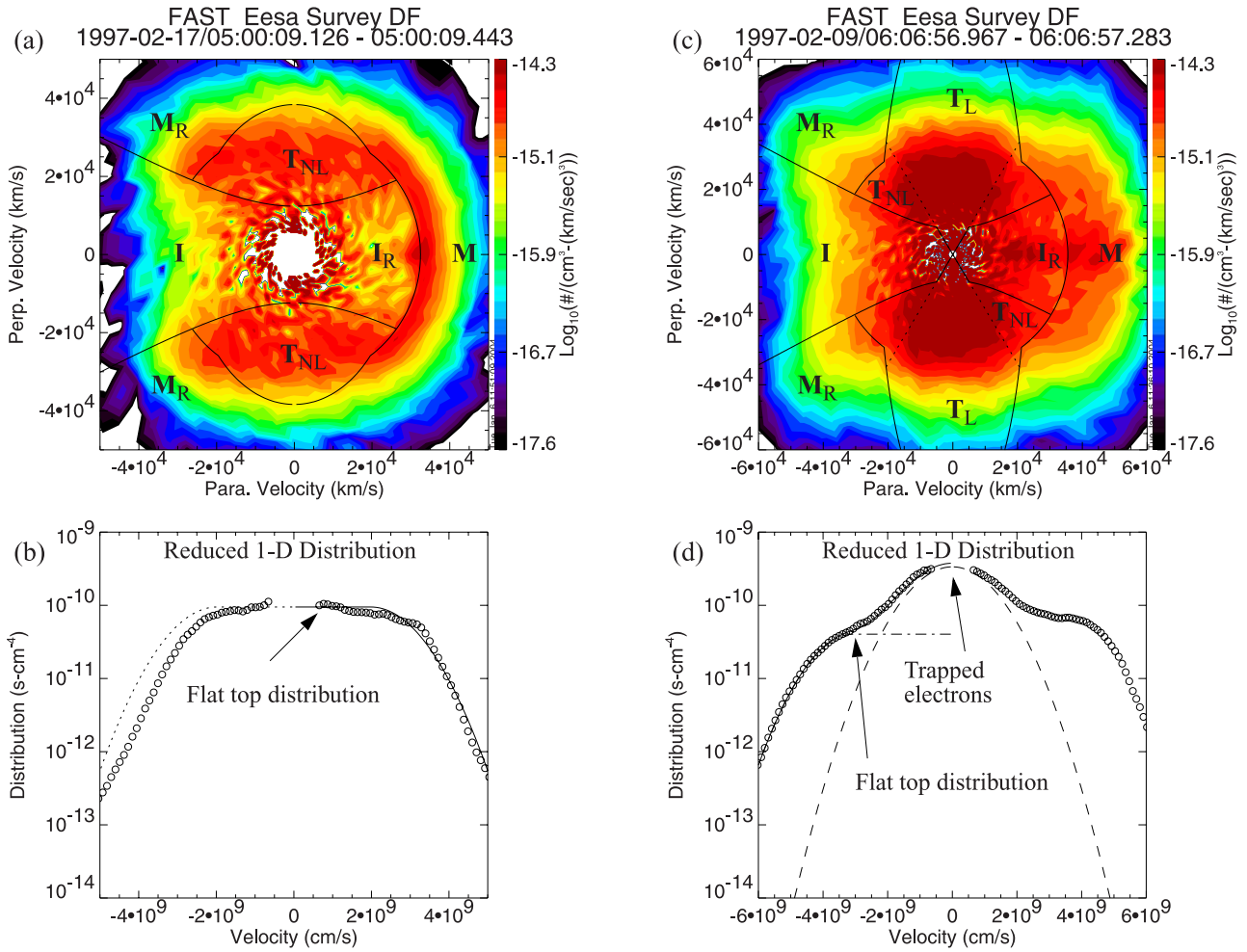

Contours on panel (a):

- Drawn for 4000 km altitude above low-altitude potential.
- $\Delta\Phi_L$ = 1600 V; Low-altitude potential drop located at 4000 km.
- $\Delta\Phi_H$ = 2000 V; High-altitude potential located at 1 R_E.
- $\Delta\Phi_M$ = 1000 V; High-altitude pre-acceleration distributed from 1 R_E to 4 R_E.

Key:

M - Electrons of magnetospheric origin.
I - Electrons of magnetospheric origin.
$\mathbf{T_L}$ - Locally trapped electrons.

Contours on panel (c):

- Drawn for 4000 km altitude below mid-cavity potential.
- $\Delta\Phi_L$ = 600 V; Low-altitude potential drop located at 3000 km.
- $\Delta\Phi_M$ = 1400 V; Mid-cavity potential located at 4250 km.
- $\Delta\Phi_H$ = 2000 V; High-altitude potential located above 1 R_E.

$\mathbf{M_R}$ - Magnetospheric electrons reflected by mirroring.
$\mathbf{I_R}$ - Ionospheric electrons reflected by high-altitude potential.
$\mathbf{T_{NL}}$ - Trapped (non-locally) by mirroring below low-altitude potential.

Figure 7. Auroral cavity electron distributions measured by the FAST satellite. (a) A 2-D plot of the electron distribution measured immediately antiearthward of a parallel electric field at the auroral cavity-ionosphere boundary. (b) The reduced, 1-D distribution from above. (c) A 2-D plot of the electron distribution measured immediately earthward of a midcavity parallel electric field. (d) The reduced, 1-D distribution from above.

mirror below the auroral cavity–ionosphere potential, and the region marked T_L are trapped electrons that mirror locally (above the auroral cavity–ionosphere potential). These boundaries are calculated assuming the conditions described in the figure.

[36] The distribution in Figure 7a (same event as in Figure 6f) appears to be from immediately antiearthward of the auroral cavity–ionosphere boundary (that is, inside the auroral cavity). The accelerated electrons of magnetospheric origin (M) are well evolved in pitch angle, indicating that it is well separated from a higher-altitude potential drop. The trapped electron population is limited to electrons that mirror below the auroral cavity–ionosphere boundary and have a relatively moderate phase-space density. The reduced, 1-D distribution (Figure 7b) fits well to a flat top (equation (1)).

[37] The electron distribution in Figure 7c (same event as in Figure 6d) is consistent with a distribution that is earthward of but close to a midcavity $E_{||}$. The accelerated electrons (M)

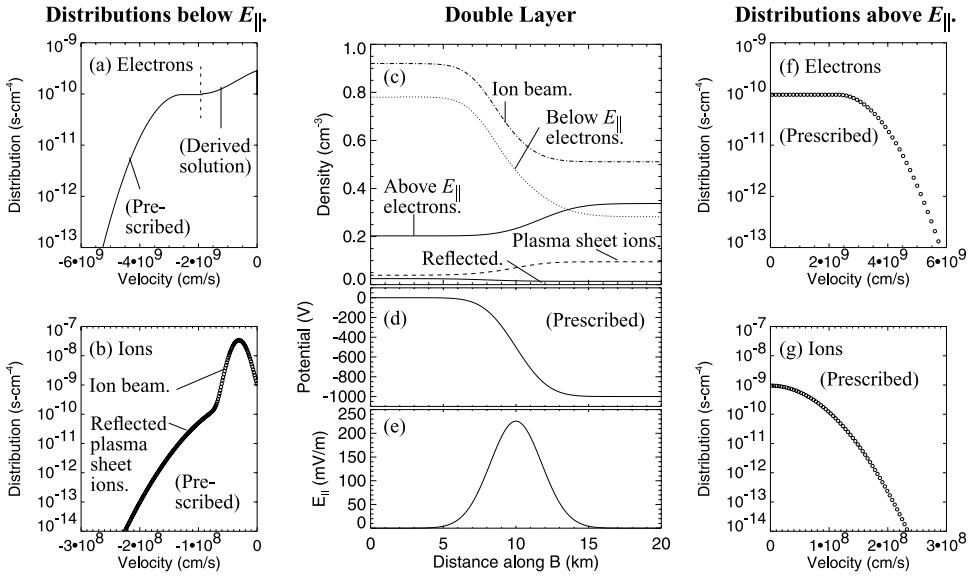

Figure 8. A midcavity double-layer solution applicable to the $E_{\|}$ event in Figure 5. (a) The prescribed (>1000 V) and derived (≤1000 V) electron distributions below (in altitude) the $E_{\|}$ event. (b) The prescribed ion distribution. This distribution has two components, an ion beam and reflected plasma sheet ions. (c) The densities of the electron and ion distributions as they evolve through the double layer. (d) The prescribed potential. (e) The prescribed $E_{\|}$ was modeled after the observations in Figure 5. (f) The prescribed electron distribution above (in altitude) $E_{\|}$. (g) The prescribed ion distribution above (in altitude) $E_{\|}$.

have only moderately evolved in pitch angle. The trapped electron populations (T_{NL} and T_L), in particular the locally trapped electrons (mirroring above the auroral cavity–ionosphere boundary), have a very high phase-space density. The trapped population contributes a significant density enhancement. The reduced 1-D distribution fits well to a "flat-top" distribution combined with a Maxwellian core (Figure 7d). The primary difference between the distribution in Figure 7a from that in Figure 7c is the phase-space density of the trapped electron population. We show that the buildup of trapped electrons within the auroral cavity allows for double layer solutions.

4.3. Double Layer Solutions

[38] Using the general characteristics (fits) of the measured distributions, we explore the possibility and determine the necessary conditions for midcavity double-layer formation. There is extensive literature on double layers (see *Raadu* [1989] for review), so we do not detail the numerous theoretical treatments of double layers.

[39] The basic approach that we use is described by *Ergun et al.* [2003]. A monotonic potential, $\Phi(z)$, is specified in a time-stationary, 1-D spatial system (z is the distance along **B**). All but one distribution (f_r, representing the reflected electrons) are specified above and below $E_{\|}$. The specified distributions are f_e^a, f_i^a, f_e^b, and f_i^b, representing the above and below $E_{\|}$ distributions (designated by superscript) and electron and ion distributions (designated by subscript). The specified distributions are assumed to satisfy the Vlasov equation. The individual charge densities can be determined as a function of position (z) through the double layer:

$$\rho_\alpha(z) = q_\alpha \int f_\alpha(\xi_\alpha(z)) \left(\frac{\partial \xi_\alpha}{\partial v}\right)^{-1} d\xi_\alpha \tag{3}$$

where v is the velocity in the z direction. Energy is defined as

$$\xi_\alpha(z) = q_\alpha \Phi(z) + \frac{1}{2} m_\alpha v^2 \tag{4}$$

where m_α and q_α are, respectively, the mass and charge of species α. A remainder function, $g(z)$ is defined as

$$g(z) = \varepsilon_o \nabla^2 \Phi(z) + \rho_e^a(z) + \rho_i^a(z) + \rho_e^b(z) + \rho_i^b(z) \tag{5}$$

[40] To satisfy Poisson's equation, the reflected distribution (f_r) is must obey the relation

$$q_r \int f_r(\xi_r(z)) \left(\frac{\partial \xi_r}{\partial v}\right)^{-1} d\xi_r = -g(z) \tag{6}$$

Once $g(z)$ is determined, equation (6) is inverted numerically to solve for f_r. A physical solution must satisfy $f_r(z, v) \geq 0$, $\forall(z, v)$.

[41] The double-layer solutions that we present here are based on Polar and FAST observations in Figures 4 and 5. The electron and ion distributions are restricted to have the forms described in equations (1) and (2). Flat-top distributions are used for magnetospheric electrons and Maxwellian distributions are used for magnetospheric ions. The anti-earthward ion beam is modeled as a drifting Maxwellian. The double-layer electric fields are fixed as Gaussian structures, restricting our analysis to monotonic potentials. The functional forms and selection of densities, drift velocities, and temperatures for each of the species can be justified on the basis of the observations. However, these parameters are adjusted to satisfy charge neutrality at the boundaries and so that solutions can be found.

[42] Figure 8 displays a midcavity double-layer solution that is based on the observations in Figures 5, 6, and 7.

Table 1. Prescribed Distributions in Figure 8

Species	Type of Fit	Density,[a] cm^{-3}	Temperature, eV	χ, eV	Drift (v_d/v_{th})
Below $E_{\|}$: Ion beam	drifting Maxwellian	0.92	125	...	2.00
Below $E_{\|}$: Reflected plasma sheet ions	Maxwellian	0.03	2500	...	...
Below $E_{\|}$: Electrons (>1000 eV)	flat top (equation (1))	...	...	300	2.50
Above $E_{\|}$: Plasma sheet ions	Maxwellian	0.06	2500	...	...
Above $E_{\|}$: Electrons	flat top (equation (1))	0.34	...	500	1.75

[a]In Tables 1–3, density represents the part of distribution drifting into region from a boundary. Reflected particles can add to the density at the boundary.

However, the measured distributions were derived from different flux tubes and do not map exactly to each other, so the fit parameters are modified to satisfy a mapping through a parallel electric field. The functional forms of the distributions are described in Table 1. The distributions f_e^a, f_i^a, and f_i^b are prescribed (only the part of a distribution moving toward the double layer is used). The high-energy (>1000 V) part of f_e^b is also prescribed. $E_{\|}$ is modeled as a Gaussian to give a 1000-V potential. The reflected part of f_e^b ($\leq$1000 V) is a numerically calculated solution of the Vlasov-Poisson equations as described in equations (3)–(6).

[43] The results in Figure 8 represent a family of double-layer solutions that are in accordance with the general characteristics of measured distributions and potential structures in the auroral cavity. The derived solution of the electron distribution below $E_{\|}$ (Figure 8a) indicates enhanced phase-space density of low-energy electrons, which is also a feature of the observed distributions. The enhanced phase space density comes from electrons trapped inside of the auroral cavity (Figure 7).

[44] Midcavity solutions requiring an enhanced trapped population were obtained with a variety of prescribed potentials and distributions under the conditions that (1) the ion beam dominates the ion density and (2) the net potential ($\Delta\Phi$) is less than the second moments of the prescribed electron distributions and high-altitude ion distributions. In other words, the double layer is "weak" with respect to the high-altitude populations but can be strong or weak with respect to the ion beam. These findings leave open the possibility that the midcavity auroral potential is held in a series of weak double layers [*Böstrom et al.*, 1988]. Since Viking spacecraft observations indicate that weak double layers do not carry sufficient potential to account for the majority of the auroral potential [*Malkki et al.*, 1993], the midcavity potential must be a minor fraction.

5. Double Layers in a Plasma-Sheet-Dominated Plasma

[45] Using the fitted forms of the measured electron and ion distributions, we explore for double-layer solutions at the magnetosphere–auroral cavity transition layer. The electron and ion distributions have the same functional form (see equations (1) and (2)) but lower densities. The primary difference between the magnetosphere–auroral cavity problem (Figures 9 and 10) and the midcavity problem (Figure 8) is that the ion density is dominated by plasma sheet ions on the high-altitude (above $E_{\|}$) side of the double layer.

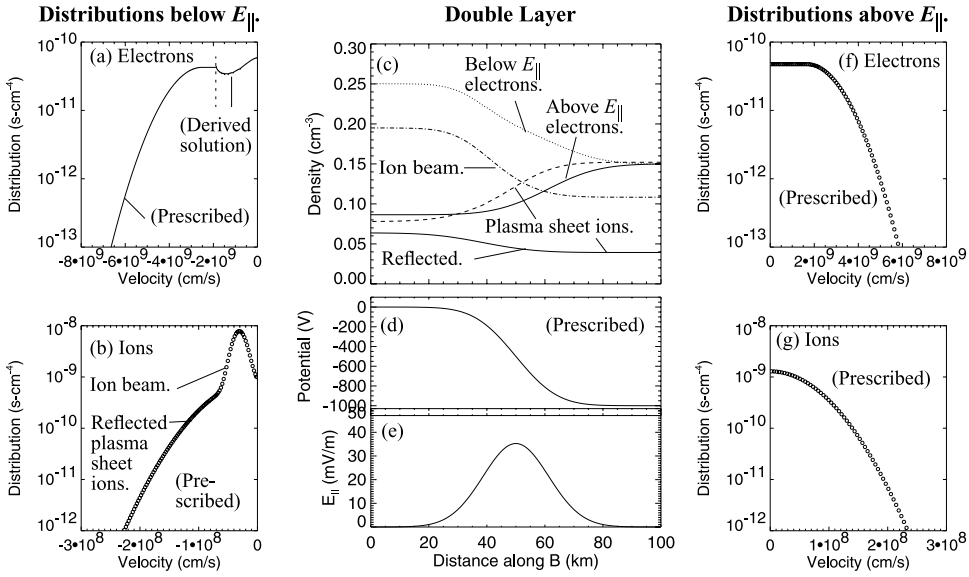

Figure 9. A plasma-sheet-dominated double-layer solution in which the magnetospheric ion density dominates above the double layer. (a) The prescribed (>1000 V) and derived ($\leq$1000 V) electron distributions below the $E_{\|}$ event. (b) The prescribed ion distribution. This distribution has two components, an ion beam and reflected plasma sheet ions. (c) The densities of the electron and ion distributions as they evolve through the double layer. (d) The prescribed potential. (e) The prescribed $E_{\|}$. (f) The prescribed electron distribution above $E_{\|}$. (g) The prescribed ion distribution above $E_{\|}$.

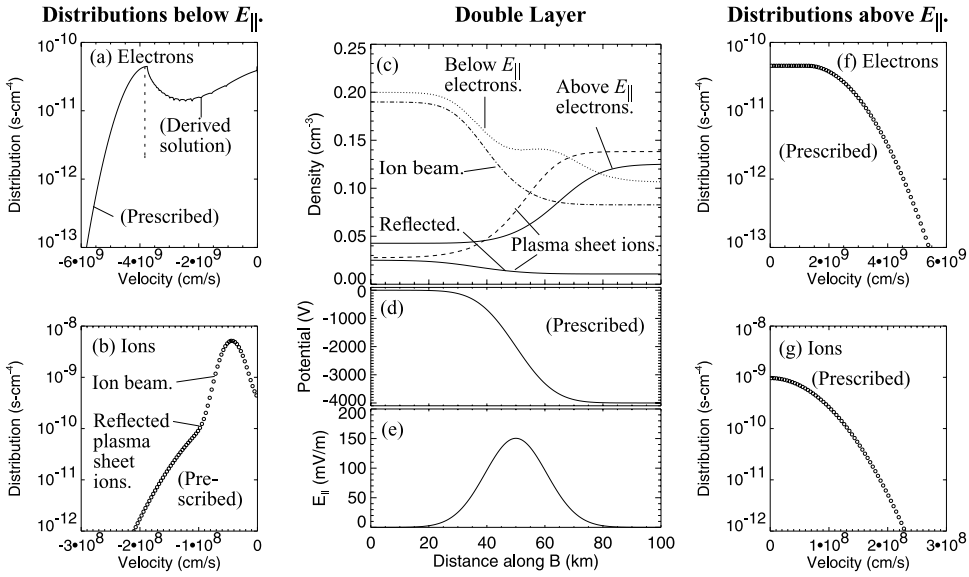

Figure 10. A plasma-sheet-dominated double-layer solution where the magnetospheric ion density dominates above the double layer. (a) The prescribed (>5000 V) and derived ($\leq$5000 V) electron distributions below the $E_\parallel$ event. (b) The prescribed ion distribution. This distribution has two components, an ion beam and reflected plasma sheet ions. (c) The densities of the electron and ion distributions as they evolve through the double layer. (d) The prescribed potential. (e) The prescribed $E_\parallel$. (f) The prescribed electron distribution above $E_\parallel$. (g) The prescribed ion distribution above $E_\parallel$.

[46] Figure 9 displays a plasma-sheet-dominated double layer solution with a 1-kV potential (Φ_{DL}). The format of the display is the same as that of Figure 8. The parameters of the prescribed distributions are in Table 2. In this example, the hot plasma sheet ions (high-altitude ions) have a higher density than the ion beam on the high-altitude side of the double layer. Essentially, the double layer forms a boundary between a region dominated by hot ions from the plasma sheet and the ion-beam-dominated region of the auroral cavity. The derived electron distribution (Figure 9a) shows a depletion in phase-space density at energies less than $e\Phi_{DL}$ (1 keV); such a distribution would be unstable. Unstable distributions emerging from a double layer have been observed in the downward current region of the aurora [*Ergun et al.*, 2000; *Andersson et al.*, 2002], so these high-altitude double-layer solutions cannot be ruled out on this basis. Furthermore, these solutions predict intense wave emissions associated with double layers which are often observed (e.g., Figure 5a).

[47] Figure 10 displays another plasma-sheet-dominated double layer solution. The characteristics of the prescribed distributions are in Table 3. The potential is fixed at higher potential (5 kV), and, as in Figure 9, the hot plasma sheet ions (above $E_\parallel$) have a higher density than the ion beam on the high-altitude side of the double layer. The depletion of phase-space density at energies less than $e\Phi_{DL}$ is much more severe, resulting is a highly unstable electron distribution (Figure 10a). Again, one would expect such a double layer to be accompanied by intense plasma waves.

[48] It is not known if any of the midcavity or plasma-sheet-dominated double layer solutions that we have presented are stable, but the BGK analysis brings out several interesting points. The ion beam-dominated solutions (Figure 8) require an enhanced trapped electron population. This population is observed to increase with increasing altitude, more accurately, with increasing distance from the auroral cavity–ionosphere boundary (Figure 7). When sufficiently developed, the trapped population provides a source of low-energy electrons that reflect at the double layer and are needed to satisfy a general Bohm condition $d\rho/d\Phi < 0$ (see *Raadu* [1989] for review), where ρ is the charge density and Φ is the potential. Thus a series of ion-beam double layers, possibly strong to the ion beam but weak to all other species, can maintain charge neutrality inside of the auroral cavity [*Mozer et al.*, 1998; *Ergun et al.*, 2000].

[49] The plasma-sheet-dominated double-layer solutions, however, require a depletion of trapped electrons. Such a depletion has not been observed and is unlikely to endure for long periods since velocity-space diffusion of electrons

Table 2. Prescribed Distributions in Figure 9

Species	Type of Fit	Density, cm^{-3}	Temperature, eV	χ, eV	Drift (v_d/v_{th})
Below $E_\parallel$: Ion beam	drifting Maxwellian	0.195	125	...	2.00
Below $E_\parallel$: Reflected plasma sheet ions	Maxwellian	0.064	4000	...	...
Below $E_\parallel$: Electrons (>1000 eV)	flat top (equation (1))	...	...	800	1.50
Above $E_\parallel$: Plasma sheet ions	Maxwellian	0.100	4000	...	...
Above $E_\parallel$: Electrons	flat top (equation (1))	0.150	...	800	1.00

Table 3. Prescribed Distributions in Figure 10

Species	Type of Fit	Density, cm^{-3}	Temperature, eV	χ, eV	Drift (v_d/v_{th})
Below $E_{\|}$: Ion beam	drifting Maxwellian	0.190	250	...	2.00
Below $E_{\|}$: Reflected plasma sheet ions	Maxwellian	0.025	4000	...	...
Below $E_{\|}$: Electrons (>1000 eV)	flat top (equation (1))	...	...	200	4.50
Above $E_{\|}$: Plasma sheet ions	Maxwellian	0.075	4000	...	...
Above $E_{\|}$: Electrons	flat top (equation (1))	0.125	...	800	0.75

is likely to rapidly increase the population of trapped electrons, leading to a breakup of a plasma-sheet-dominated double layer.

6. Discussion and Conclusions

[50] Polar and Fast observations support the possibility that the strong double layer is the dominant physical mechanism that supports the parallel electric fields at the auroral cavity–ionosphere boundary. The observations show an abrupt onset of the ion beam, an abrupt decrease in electron energy, a sharp drop in plasma density, and strong electric field signatures as the spacecraft crosses the auroral cavity–ionosphere boundary. These observations, along with the direct observations of the parallel electric fields, are strong evidence of the existence of strong double layers.

[51] The double layers at the auroral cavity–ionosphere boundary are generally oblique with $E_{\perp} > E_{\|}$. The auroral cavity can extend for $O(10^4)$ km in altitude, whereas the region extends $O(10^2)$ in latitude, so parallel electric fields are expected to be observed for only a fraction the auroral cavity–ionosphere boundary crossings. While not conclusive, observational occurrence of oblique double layers supports the possibility that the double layer is a primary acceleration mechanism at the low-altitude boundary.

[52] Stationary double-layer solutions are possible because of the heated ions that are accelerated by the magnetic mirror force and are drifting antiearthward. The ion heating in the upward current region of the ionosphere is from wave modes excited by the accelerated electrons so, once established, the stationary oblique double layer is self-supporting.

[53] The parallel electric field at the auroral cavity–ionosphere boundary is required for quasi-neutrality inside of the auroral cavity. The upward current region ionosphere has not only a cold electron population but also scattered and secondary electrons and mirroring electrons that result from the electron acceleration. The latter electron populations have much higher energies than any of the ionospheric ion species and much higher densities than the magnetospheric species. In the absence of a retarding electric field, these electrons would overwhelm the auroral cavity.

[54] The quasi-neutral condition within the auroral cavity requires a balance between the electrons and ions emerging from the auroral cavity–ionosphere boundary, the electrons and ions emerging from the auroral cavity–magnetosphere boundary, and the trapped electron population. The trapped electrons result from velocity-space diffusion and can account for a significant fraction if not the majority of the electron density. The trapped population appears to play an important role in determining the spatial distribution of the auroral potential.

[55] We have presented observations from Polar and FAST of two possible examples of midcavity or ion-beam double layers. The observed $E_{\|}$ signals reach a relatively high amplitude (70 mV/m in the Polar example, 250 mV/m in the FAST example) and endure for short <1-s periods (or have finite spatial extents; Figures 4 and 5). The observed midcavity double layers are associated with intense wave turbulence. The speed of the structures along **B** is not known, so the parallel sizes of the structures cannot be determined from electric field observations alone. However, the potential can be estimated from the changes in the ion distributions, implying sizes of the order of 10 λ_D. Numerical solutions of these structures indicate that the observed electron and ion distributions and the electric field signal are consistent with an ion-beam double layer. These double layers can be considered weak double layers ($\Delta\Phi < T_{\|}$) for all species except for the ion beam. $\Delta\Phi$ can be greater than $T_{\|}$ of the ion beam.

[56] The observations and analysis presented in this paper suggest that midcavity or ion-beam double layers can develop with a buildup of trapped electrons. The buildup of trapped electrons requires a significant distance (mirror ratio) from the auroral cavity–ionosphere boundary. The observations also suggest that multiple double layers may lie on the same magnetic flux tube. The ion-beam double layers appear to have potentials that are a minority fraction of the total auroral potential. This fact, combined with the possibility of an oblique double layer at the auroral cavity–ionosphere boundary suggests that the total auroral potential is contained in a series of potential drops, at least some of which are discrete double layers.

[57] The majority of the electron acceleration in the upward current region is known to occur above $\sim$1 R_E in altitude [*Reiff et al.*, 1993]. At these altitudes, the density of the magnetospheric ions exceeds the ion-beam densities. BGK solutions were explored using a restricted set of boundary distributions, a Gaussian potential form, and a dominant magnetospheric ion density on the high-altitude side of the double layer. Under these restrictions, the solutions predict that the electron distribution in the auroral cavity has strong depletion in phase-space density at low energies. Such distributions are highly unstable, but double-layer solutions cannot be ruled out on that basis. However, electron distributions in the auroral cavity can experience velocity space diffusion from the plasma waves and should build up a trapped population. A buildup of trapped electrons would not be consistent with the restricted set of high-altitude BGK solutions that we have explored.

[58] We point out that neither nonmonotonic double-layer solutions nor moving double-layer solutions have been explored in this study. The self-consistent solution of the plasma-sheet-dominated auroral acceleration remains an open question that needs to be resolved. Trapped electrons,

moving potential structures, nonmonotonic potential structures, and intense electrostatic turbulence may play a large role.

[59] **Acknowledgments.** This article was supported by NASA grants NAG5-12026, NAG5-3596 (FAST), and NAG5- 3182 (Polar), and by NSF grants ATM-0202564 and ATM-0206906.

[60] Shadia Rifai Habbal thanks both referees for their assistance in evaluating this paper.

References

Andersson, L., R. E. Ergun, D. L. Newman, J. P. McFadden, C. W. Carlson, and Y.-J. Su (2002), Characteristics of parallel electric fields in the downward region on the aurora, *Phys. Plasmas*, *9*, 3600.

Block, L. P. (1972), Potential double layers in the ionosphere, *Cosmic Electrodyn.*, *3*, 349.

Block, L. P., C.-G. Falthammar, P.-A. Lindqvist, G. Marklund, and F. S. Mozer (1987), Electric field measurements on Viking: First results, *Geophys. Res. Lett.*, *14*, 435.

Böstrom, R., G. Gustafsson, B. Holback, G. Holmgren, and H. Koskinen (1988), Characteristics of solitary waves and weak double layers in the magnetospheric plasma, *Phys. Rev. Lett.*, *61*, 82.

Burch, J. L. (1988), Simultaneous plasma observations with DE-1 and DE-2, *Adv. Space Res.*, *8*, 353.

Carlson, C. W., R. Pfaff, and J. G. Watzin (1998), The Fast Auroral Snapshot (FAST) mission, *Geophys. Res. Lett.*, *25*, 2013.

Chaston, C. C., J. W. Bonnell, J. P. McFadden, R. E. Ergun, and C. W. Carlson (2002), Electromagnetic ion cyclotron waves at proton cyclotron harmonics, *J. Geophys. Res.*, *107*(A11), 1351, doi:10.1029/2001JA900141.

Ergun, R. E., et al. (1998), FAST satellite wave observations in the AKR source region, *Geophys. Res. Lett.*, *25*, 2061.

Ergun, R. E., C. W. Carlson, J. P. McFadden, F. S. Mozer, and R. J. Strangeway (2000), Parallel electric fields in discrete arcs, *Geophys. Res. Lett.*, *27*, 4053.

Ergun, R. E., L. Andersson, D. Main, Y.-J. Su, D. L. Newman, M. V. Goldman, C. W. Carlson, J. P. McFadden, and F. S. Mozer (2002a), Parallel electric fields in the upward current region of the aurora: Indirect and direct observations, *Phys. Plasmas*, *9*, 3685.

Ergun, R. E., L. Andersson, D. Main, Y.-J. Su, D. L. Newman, M. V. Goldman, C. W. Carlson, J. P. McFadden, and F. S. Mozer (2002b), Parallel electric fields in the upward current region of the aurora: Numerical solutions, *Phys. Plasmas*, *9*, 3695.

Evans, D. S. (1974), Precipitation electron fluxes formed by a magnetic-field-aligned potential difference, *J. Geophys. Res.*, *79*, 2853.

Fridman, M., and J. Lemaire (1980), Relationship between auroral electrons fluxes and field aligned electric potential difference, *J. Geophys. Res.*, *85*, 664.

Gavrishchaka, V. V., G. I. Ganguli, W. A. Scales, S. P. Slinker, C. C. Chaston, J. P. McFadden, R. E. Ergun, and C. W. Carlson (2000), Multiscale coherent structures and broadband waves due to parallel inhomogeneous flows, *Phys. Rev. Lett.*, *85*, 4285.

Haerendel, G., E. Rieger, A. Valenzuela, H. Foeppl, H. C. Stenbaek-Nielsen, and E. M. Wescott (1976), First observation of electrostatic acceleration of barium ions into the magnetosphere, in *ESA European Programmes on Sounding-Rocket and Balloon Research in the Auroral Zone*, pp. 203–211, Eur. Space Agency, Paris.

Hudson, M. K., and F. S. Mozer (1978), Electrostatic shocks, double layers, and anomalous resistivity in the magnetosphere, *Geophys. Res. Lett.*, *5*, 131.

Hull, A. J., J. W. Bonnell, F. S. Mozer, and J. D. Scudder (2003a), A statistical study of large-amplitude parallel electric fields in the upward current region of the auroral acceleration region, *J. Geophys. Res.*, *108*(A1), 1007, doi:10.1029/2001JA007540.

Hull, A. J., J. W. Bonnell, F. S. Mozer, J. D. Scudder, and C. C. Chaston (2003b), Large parallel electric fields in the upward current region of the aurora: Evidence for ambipolar effects, *J. Geophys. Res.*, *108*(A6), 1265, doi:10.1029/2002JA009682.

Ishiguro, S., et al. (1997), V-shaped dc potential structure caused by current-driven electrostatic ion-cyclotron instability, *Phys. Rev. Lett.*, *78*, 4761.

Klumpar, D. M. (1979), Relationships between auroral particle distributions and magnetic field perturbations associated with field-aligned currents, *J. Geophys. Res.*, *84*, 6524.

Knight, S. (1973), Parallel electric fields, *Planet. Space Sci.*, *21*, 741.

Maggs, J. E. (1976), Coherent generation of VLF hiss, *J. Geophys. Res.*, *81*, 1707.

Malkki, A., A. I. Eriksson, P.-O. Dovner, R. Bostrom, B. Holback, G. Holmgren, and H. E. J. Koskinen (1993), A statistical survey of auroral solitary waves and weak double layers: 1. Occurrence and net voltage, *J. Geophys. Res.*, *98*, 15,521.

McIlwain, C. E. (1960), Direct measurements of particles producing visible auroras, *J. Geophys. Res.*, *65*, 73.

Mozer, F. S., and A. Hull (2001), Origin and geometry of upward parallel electric fields in the auroral acceleration region, *J. Geophys. Res.*, *106*, 5763.

Mozer, F. S., and C. A. Kletzing (1998), Direct observation of large, quasi-static, parallel electric fields in the auroral acceleration region, *Geophys. Res. Lett.*, *25*, 1629.

Mozer, F. S., C. W. Carlson, M. K. Hudson, R. B. Torbert, B. Parady, J. Yatteau, and M. C. Kelley (1977), Observations of paired electrostatic shocks in the polar magnetosphere, *Phys. Rev. Lett.*, *38*, 292.

Raadu, M. A. (1989), The physics of double layers and their role in astrophysics, *Phys. Rep.*, *178*, 25.

Reiff, P. H., H. L. Collin, J. D. Craven, J. L. Burch, J. D. Winningham, E. G. Shelley, L. A. Frank, and M. A. Friedman (1988), Determination of auroral electrostatic potentials using high- and low-altitude particle distributions, *J. Geophys. Res.*, *93*, 7441.

Reiff, P. H., G. Lu, J. L. Burch, J. D. Winningham, L. A. Frank, J. D. Craven, W. K. Peterson, and R. A. Heelis (1993), On the high- and low-altitude limits of the auroral electric field region, in *Auroral Plasma Dynamics*, *Geophys. Monogr. Ser.*, vol. 80, edited by R. L. Lysak, p. 143, AGU, Washington, D. C.

Roth, I., M. K. Hudson, and R. Bergmann (1989), Effects of ion two-stream instability on auroral ion heating, *J. Geophys. Res.*, *94*, 348.

Schamel, H., and S. Bujarbarua (1983), Analytical double layers, *Phys. Fluids*, *26*, 190.

Shelley, E. G., R. D. Sharp, and R. G. Johnson (1976), Satellite observations of an ionospheric acceleration mechanism, *Geophys. Res. Lett.*, *3*, 654.

Strangeway, R. J., et al. (1998), FAST observations of VLF waves in the auroral zone: Evidence of very low plasma densities, *Geophys. Res. Lett.*, *25*, 2065.

Temerin, M., K. Cerny, W. Lotko, and F. S. Mozer (1982), Observations of double layers and solitary waves in the auroral plasma, *Phys. Rev. Lett.*, *48*, 1175.

L. Andersson, R. E. Ergun, D. Main, and Y.-J. Su, Laboratory for Atmospheric and Space Physics, University of Colorado, Boulder, CO 80303, USA. (ree@fast.colorado.edu)

C. W. Carlson, A. J. Hull, J. P. McFadden, and F. S. Mozer, Space Sciences Laboratory, University of California, Berkeley, Berkeley, CA 80303, USA.

M. V. Goldman and D. L. Newman, Center for Integrated Plasma Studies, University of Colorado, Boulder, CO 94720, USA.